Extracellular gradient amplification by eukaryotic cells and power-law scaling in screened gradients

Igor Segota and Carl Franck
Laboratory of Atomic and Solid State Physics, Cornell University, Ithaca, NY 14853, USA
[submitted to PLoS ONE]

Cells can sense and respond to very weak, but sometimes vital signals in the form of shallow chemical gradients. It was recently suggested that single cells can amplify such weak signals by secreting degradatory enzymes which act to effectively screen the gradient and could possibly steepen the local gradient perceived by single cells. However this effect was largely ignored in study of cell chemotaxis. Here we revisit this effect with a focus on a well described *Dictyostelium discoideum* cAMP chemotaxis system where cAMP signals are affected by an extracellular cAMP phosphodiesterase (PDE) and its inhibitor (PDI). Using a reaction-diffusion model of this set of interactions in the extracellular space, we show that cells can effectively sense much steeper chemical gradients than naively expected (up to a factor of 12). Next, we find that the rough estimates of experimental PDE and PDI secretion rates are close to the optimal values predicted by our model. Finally, we find that the cAMP screening length exhibits power-law scaling with both PDE and PDI secretion rates and discuss how these results could be experimentally tested.

INTRODUCTION

Living cells must often sense and respond to extracellular signals in the form of chemical gradients. In contrast to temporal gradient sensing typical for small bacteria such as *E.coli* [1], larger eukaryotic cells are able to sense chemical gradients directly [2]. Well studied examples of eukaryotic gradient sensing studies include chemotaxis in *Dictyostelium discoideum* amoebae, neutrophils [3] and tumor cells [4, 5] or chemotropic growth in *Saccharomyces cerevisiae*. Due to its important role in life functions such as organ formation, wiring of the nervous system, wound healing and cancer, chemotaxis has become a tremendous area of research [4, 5].

Eukaryotic cells are often found to secrete enzymes that inactivate or degrade the chemical signal in the extracellular space. In particular, during cAMP (cyclic adenosine monophosphate) chemotaxis *D. discoideum* cells secrete cAMP phosphodiesterase [6], neutrophils can inactivate chemotactic formylmethionyl peptides [3] and *S. cerevisiae* cells secrete Bar1 protease that degrades α-factor pheromone signals that guide their growth towards their mating partners. In addition to PDE, *D. discoideum* cells secrete a PDE inhibitor (PDI) [7].

One function of enzymes such as PDE or Bar1 is to lower the extracellular signal concentration, which is useful if the signal concentration would saturate its receptors. More recently, it has been suggested that these inactivating enzymes have the additional function to amplify the signal by steepening its chemical gradient in *D. discoideum* ([8], p.125) or to improve the alignment of the gradient direction with the nearest mating partner in *S. cerevisiae* [9–11]. Barkai et al.[9] argued that the mechanism of signal degradation resembles electrostatic screening by noting the analogy between steady-state diffusion equation and Laplace equation for the electrostatic potential, but that in the case of *S. cerevisiae* this effect does not provide an advantage when there is only one mating partner.

In *D. discoideum* cAMP signals are relayed between cells during the aggregation stage however to date, little effort has been made to explain and quantify how the combined effect of PDE and PDI exactly affects the local cAMP gradient perceived by each *D. discoideum* cell. On the contrary, Nanjundiah and Malchow [12] argued using dimensional analysis, that the extracellular PDE serves no purpose in cAMP signaling involved in cell aggregation. More recently, authors in [13–15] investigated the role of extracellular PDE and PDI in the model of dynamical wave pattern formation and argued that within the particular parameter range of their model, PDE becomes important for aggregation at lower cell densities [13, 14] and PDI becomes important in the formation of spiraling wave patterns [15].

Experimentally, *D. discoideum* strains with inactive PDE gene (PDE-null cells) have been shown to fail to aggregate [16, 17], while strains with inactive PDI gene are slow to aggregate and fail to produce spiral cAMP waves [15], which are critical for establishing suitably large aggregation territories. The difficulty with interpreting the results from experiments with PDE-null cells stems from the fact that the same gene codes for both the extracellular and the membrane-bound form of this enzyme. This makes it difficult to distinguish between the effects of each PDE form on the cAMP gradient. While these earlier experiments with inactivated PDE and PDI [15–17] are biologically relevant and imply PDE and PDI may have roles in establishing spiral wave patterns, they do not provide much quantitative insight into how the biochemical reactions between cAMP, PDE and PDI affect the cAMP gradient perceived by cells. For example, if the extracellular PDE concentration doubles, how does the gradient or cell response scale?

In this work, we focus on well characterized *D. discoideum* gradient sensing and address this effect by developing two models predicting the effective cAMP concentration profile and its gradient, as a result of its interactions with PDE and PDI. The models are centered around a set of six reaction-diffusion equations for six chemical species: cAMP, PDE, PDI, cAMP-PDE complex, PDE-PDI complex and 5'AMP, a product of cAMP-PDE reaction. The calculations are done for experimentally directly testable scenarios where static cAMP gradients can be set up by diffusion in agarose-based microfluidic devices [18–20], but the gradients can be af-

fected by enzymes such as PDE or PDI. In one scenario we assumed a uniform PDE concentration and no PDI, and in another scenario we consider a more practical case where both PDE and PDI are secreted from the stationary circular cell with constant fluxes.

In other experimental arrangements employed recently [21–23], static (time-independent) flowing gradients can be set up by flow mixing where in principle anything secreted by cells is swept away and the effect of PDE and PDI would not be observed. Our discussion here casts doubt on the applicability of such experiments to limitations of gradient sensing in natural living systems.

RESULTS

Model 1. Uniform PDE concentration. As the first and simplest model we consider a system of two interacting molecules, PDE and cAMP, following Michaelis-Menten kinetics and completely ignoring PDI:

$$\mathrm{PDE} + \mathrm{cAMP} \underset{k_{-1}}{\overset{k_1}{\rightleftharpoons}} \mathrm{COMPLEX} \xrightarrow{k_2} \mathrm{PDE} + 5'\mathrm{AMP} \qquad (1)$$

where the COMPLEX represents the intermediate PDE-cAMP complex and 5'AMP the product of this reaction, which does not bind to *D. discoideum* cAMP receptors and can be considered as a deactivated signal.

In modeling the cAMP-PDE reaction, we employ the standard quasi-steady state assumption [24], which assumes the concentration of the intermediate complex does not change on the time scale of product formation $k_1 cp = (k_{-1}+k_2)C_{cp}$, where c, p and C_{cp} stand for cAMP, PDE and cAMP-PDE complex concentrations, respectively. Since here we consider the case of uniform PDE concentration, we set $p(x,t) = p_0$. Expressing all concentrations in units of the Michaelis-Menten constant $K_M \equiv (k_{-1}+k_2)/k_1$ and spatial coordinates in units of characteristic lengths $\lambda_0 = \sqrt{(DK_M)/(k_2 p_0)} \approx 13\,\mu$m (see SI), where D is the cAMP diffusion constant 444 μm^2/s [32], the cAMP equation in steady state simplifies to:

$$\nabla^2 c - c = 0 \qquad (2)$$

The Eq.2 for cAMP concetration $c(x)$ has the same form as the equation for the electrostatic Coulomb potential screened by charged particles in electrolytes [25], with the screening length λ_0. The same result was obtained previously by Barkai et al.[9]. The interpretation of this result is that it describes diffusion of cAMP molecules with fixed probability of disappearing per unit time (representing the conversion to 5'AMP), described by lifetime $\tau = K_M/(k_2 p_0) \approx 0.4\,$s and screening length λ_0 (a typical distance cAMP moves before being converted to 5'AMP).

Boundary conditions in 1D are taken as:

$$c(x=0) = c_0,\ c(x=a) = 0 \qquad (3)$$

and we set our system to span a length of ten characteristic lengths, $a = 10$. Physically, this represents a cAMP source at $x = 0$, and a drain "far" away at $x = a$. The analytical solution of Eq.2 with boundary conditions in Eq. 3 is (derivation in SI):

$$c(x) = c_0 \frac{\sinh(a-x)}{\sinh(a)}$$

For the 2D case, the solution was computed on a domain defined by the difference between the rectangular domain defined by $0 \le x \le 10\lambda_0$, $-10\lambda_0 \le y \le 10\lambda_0$ and a circle centered at $(x_0, y_0 = 0)$ with a diameter $1\,\lambda_0$, representing a cell. The boundary conditions were:

$$c(x=0,y) = c_0,\ c(x=10\lambda_0, y) = 0$$

$$(-D\nabla c)_{y=-10\lambda_0} = (-D\nabla c)_{y=10\lambda_0} = (-D\nabla c)_{circle} = 0$$

where the circular hole represents a cell impermeable to cAMP. These boundary conditions are present in typical microfluidic devices where the concentrations are experimentally set by continuously flowing fixed concentrations of cAMP through the microfluidic channels and the gradient is established by diffusion through agarose gel [18, 26]. The cAMP gradient was defined as the concentration difference between front and the back of the cell, divided by its diameter:

$$\nabla c \equiv \frac{c(x_0 - r, y_0) - c(x_0 + r, y_0)}{2r}$$

where (x_0, y_0) are the coordinates of the cell center. This definition reflects a biologically relevant quantity which is actually perceived by the cell, related to the concentration difference between its front and back (Fig. 1a).

In order to quantify a possible gradient steepening, we computed the ratio between the gradient in this model and the constant gradient that would have been established without PDE. In 1D the analytical result for this gradient ratio is:

$$\frac{\nabla c}{\nabla c_{\mathrm{noPDE}}} = \frac{a \cdot \cosh(a-x)}{\sinh(a)} \approx \frac{a e^a}{\sinh(a)} e^{-x}$$

with:

$$c_{\mathrm{noPDE}}(x) = c_0 \left(1 - \frac{x}{a}\right),\ \nabla c_{\mathrm{noPDE}} = -\frac{c_0}{a}$$

In the range $0 \le x \le a = 10$ the gradient ratio is well approximated by an exponential, as can be seen in Fig. 1. Viewing cAMP as a molecule performing a random walk with constant probability of disappearing per unit time in 1D, the probability of finding it drops exponentially as we move away from the source.

The spatial range with steeper gradient $\nabla c > \nabla c_{\mathrm{noPDE}}$ is shown in Fig.1 corresponding to $x < 10\lambda_0 - \mathrm{arccosh}[\sinh(10\lambda_0)/10\lambda_0] \approx 2.3\,\lambda_0$ where we used 5.2 nM as a typical PDE concentration value [27] (see SI for details), which gives $\lambda_0 \approx 13\,\mu$m. Therefore, this model predicts gradient steepening in the range up to about 30 μm from the cAMP source.

As the PDE concentration p_0 is changed the solution for the cAMP concentration and gradient is always qualitatively the same and the screening length scales as a power law with the PDE concentration: $\lambda_0 \sim p_0^{-0.5}$.

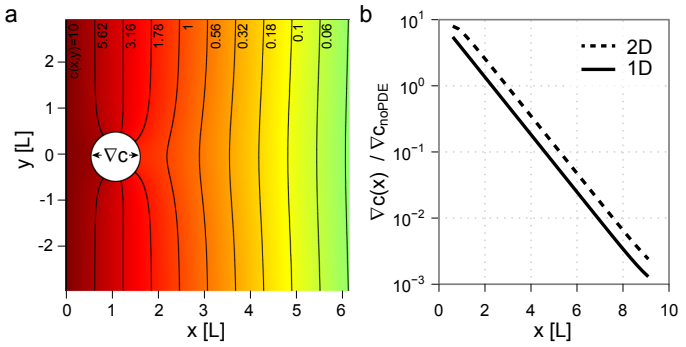

FIG. 1. a) Simulated steady state cAMP gradient on the cell, expressed as the concentration difference between front and the back of the cell, divided by its diameter. Only the range $0 \leq x/\lambda_0 \leq 6$, $-3 \lesssim y/\lambda_0 \lesssim 3$ is shown. b) The gradient ratio – cAMP gradient divided by the cAMP gradient without any PDE. The net effect of uniform PDE profile in both 1D and 2D is the gradient steepening in the range where $\nabla c > \nabla c_{\mathrm{noPDE}}$, corresponding to $x \lesssim 30\,\mu$m.

Model 2. Source of PDE and PDI. Here we give a more realistic extension of a previous 2D model, and we consider the fact that both PDE and PDI are in reality secreted by a cell. Assuming that the PDE-PDI interaction follows a first-order protein-ligand binding [7], the two sets of interactions are:

$$\mathrm{PDI} + \mathrm{PDE} \underset{k'_{-1}}{\overset{k'_1}{\rightleftharpoons}} \mathrm{COMPLEX_{ip}}$$

$$\mathrm{PDE} + \mathrm{cAMP} \underset{k_{-1}}{\overset{k_1}{\rightleftharpoons}} \mathrm{COMPLEX_{pc}} \overset{k_2}{\rightarrow} \mathrm{PDE} + 5'\mathrm{AMP}$$

Using a quasi steady state approximation $(k_{-1} + k_2)C_{pc} = k_1 cp$, expressing the concentrations in units of K_d (PDE-PDI dissociation constant) and rescaling the length with a characteristic length $x/L \to x$ ($L = \sqrt{D_c/k'_{-1}}$) the steady state form of these equations become (full derivation given in SI):

$$\nabla^2 c = Kcp \tag{4}$$

$$\frac{D_p}{D_c}\nabla^2 p = pi - C_{ip} \tag{5}$$

$$-\frac{D_{C_{ip}}}{D_c}\nabla^2 C_{ip} = pi - C_{ip} \tag{6}$$

$$\frac{D_i}{D_c}\nabla^2 i = pi - C_{ip} \tag{7}$$

where the constant K is estimated to be on the order of 1 (see SI) and D_c, D_p, $D_{C_{ip}}$, D_i are the diffusion constants of cAMP, PDE, PDE-PDI complex and PDI, respectively. The equation system was solved on a rectangular domain given by $0 \leq x \leq 10L$, $-10L \leq y \leq 10L$ (here $L = 100\,\mu$m), excluding a circle at coordinates $(x_0, y_0 = 0)$ and a radius $r = 0.05\,L$. The boundary conditions are given in Table I.

The constant PDE and PDI secretion rates were modeled as constant flux boundary conditions on the internal circular boundary with PDE and PDI fluxes defined as $-D_p\nabla p = p_0$, $-D_i\nabla i = i_0$ respectively. The model was then solved by finite element method using COMSOL with MATLAB (Comsol Inc.) by varying three parameters: cell position x_0 (distance from cAMP source) PDE flux p_0 and PDI flux i_0 (see SI for details).

The quantity of interest is the cAMP gradient ratio which tells us the factor by which the cAMP is steepened or flattened compared to the case without PDE and PDI. It is proportional to the cAMP gradient since the cAMP gradient without PDE/PDI is uniform due to the boundary conditions. The cAMP gradient ratio as a function of x_0, p_0 and i_0 is shown in Fig.2. We see that the gradient only for a ceratin values of PDE/PDI fluxes and only in some spatial range close to the cAMP source. The cAMP gradient can be steepened up to a factor of 12 when the cell is 60 μm away from the cAMP source ($x_0 = 0.6\,L$) and the steepening persists even to distances of about 200 μm away from the cAMP source. However, while the color density plot in Fig.2 shows for which combinations of x_0, p_0 and i_0, it is difficult to read out the functional dependence from colors.

The cAMP gradient ratio as a function of cell position is shown in Fig.3a-c, therefore we notice that for a wide (but not full) range of parameters the cAMP gradient is still characterized by the exponential decay in a large spatial region, similar to the screening effect found in the previous model. We also show the cAMP gradient ratio as a function of PDE and PDI in Fig.3d-f. These graphs correspond to vertical or horizontal slices through Fig.2b. Lastly, we calculated the cAMP screening lengths and their scaling as functions of PDE and PDI flux and found a power law scaling and the corresponding exponents in a certain range; see Fig.3g-i.

In the case of no PDI, the cAMP screening length scales with PDE as $\lambda \sim p_0^{-1.04}$ in low flux range or $\lambda \sim p_0^{-0.54}$ in high flux range. With PDI, in much of the range the PDE scaling is $\lambda \sim p_0^{-0.78}$, and the PDI scaling is $\lambda \sim i_0^{0.55}$ for high flux range around the experimentally estimated value.

DISCUSSION

The effect of cell size on the gradient was considered previously in a system with static gradients established in flowing microfluidic devices [28] and for non-flowing gradients in [29] and also here (see SI). For static gradients, the presence of a cell steepens the gradient by a factor of two. This effect is also shown in Fig.2b, where the cAMP gradient ratio saturates at a value of two instead of one, for small PDE and PDI fluxes.

We used the previous experimental data [27, 30] to obtain the rough estimates for PDE and PDI fluxes (see SI). We obtained $p_0^{exp} = 0.02\,K_d k'_{-1} L$ and $i_0^{exp} = 0.1\,K_d k'_{-1} L$ for PDE and PDI fluxes respectively, which are shown in Fig.2b (as circles, indicating the large uncertainty of this estimate). Based on this comparison in Fig.2b and Fig.3d-e, the PDE flux is close to the optimal value predicted by the model in a fairly large spatial region. The gradient steepening can be achieved even without PDI, and according to Fig.2b, the model predicts that varying PDI flux below i_0^{exp} does not affect the cAMP gradient perceived by cells. The PDI flux also seems to be around its optimal value as shown in Fig.3f either in the sense that it is in the most steep region of the sigmoidal curve where it can have most effect on the gradient or right at the optimal peak value at about $0.1\,K_d k'_{-1} L$. The

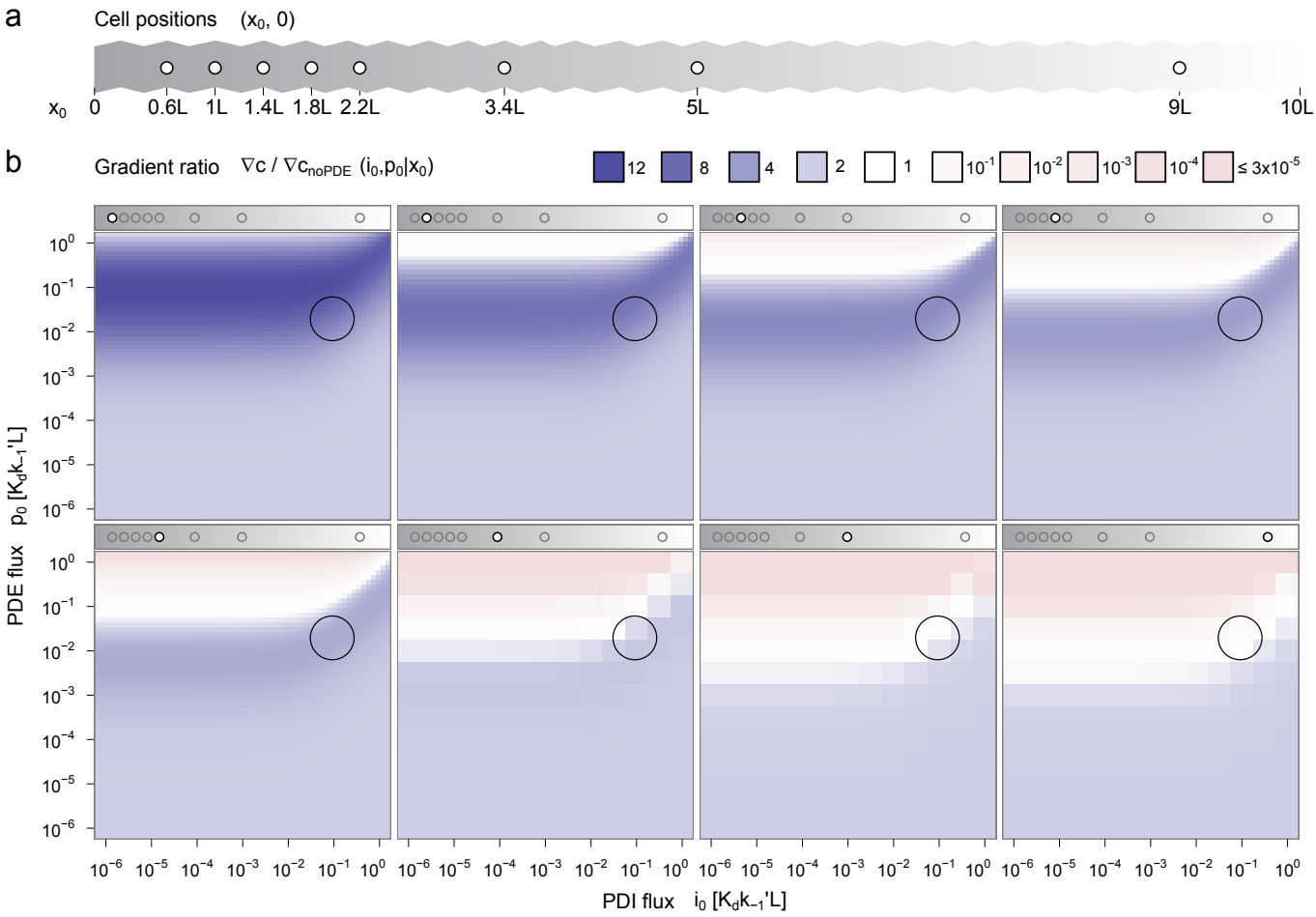

FIG. 2. a) A slice of the entire 2D domain showing the several cell positions $x_0, y_0 = 0$ chosen for the simulation, at variable distances from the cAMP source (at $x = 0$). The system size was $10L \times 20L$. b) Gradient ratio $\nabla c(x_0)/\nabla c(x_0)_{\mathrm{noPDE}}$ as a function of PDI and PDE fluxes i_0 and p_0, respectively. For each cell position x_0, we varied i_0 and p_0 across the range of six orders of magnitude. The range of combinations of x_0, i_0 and p_0 that steepen the cAMP gradient is shown in blue. The bars above each plot show the relative position of the cell x_0 with actual values given in a). The circle on each plot denotes the rough range of PDE and PDI fluxes estimated based on the data from previous experiments, with values $p_0^{exp} = 0.02\, K_d k'_{-1} L$ and $i_0^{exp} = 0.1\, K_d k'_{-1} L$ (see SI).

	Boundary conditions	cAMP $c(x,y)$	PDE $p(x,y)$	PDI $i(x,y)$	PDE-PDI complex $C_{ip}(x,y)$
left	$x = 0, y$	$c(0,y) = c_0$	$p(0,y) = 0$	$i(0,y) = 0$	$C_{ip}(0,y) = 0$
right	$x = 10L, y$	$c(10L,y) = 0$	$p(10L,y) = 0$	$i(10L,y) = 0$	$C_{ip}(10L,y) = 0$
top, bottom	$x, y = \pm 10L$	$-D_c\nabla c = 0$	$-D_p\nabla p = 0$	$-D_i\nabla i = 0$	$-D_{Cip}\nabla C_{ip} = 0$
cell	$(x-x_0)^2 + y^2 = (0.05L)^2$	$-D_c\nabla c = 0$	$-D_p\nabla p = p_0$	$-D_p\nabla p = i_0$	$-D_{Cip}\nabla C_{ip} = 0$

TABLE I. Boundary conditions for Model 2. These reflect the conditions present in a typical no-flow microfluidic device where static gradients are set by controlling concentrations of various chemical species in the two side channels (here denoted as left and right).

cells are therefore able to tune the extracellular cAMP gradient at various distances from the cAMP source, by actions of PDE and PDI.

The effects discussed here lead to different predictions between the chemotaxis responses in experiments with static non-flowing gradients where cAMP gradients are affected by secreted PDE and PDI [18–20] and the experiments with static flowing gradients set up by flow mixing [21–23] and the delicate PDE/PDI profiles are destroyed. In the light of our findings here, the results of the flowing gradient experiments should be reinterpreted.

The results from the models provided here can be further experimentally tested. Using microfluidic devices recently applied to *D. discoideum* chemotaxis [18] with static cAMP gradients, one can measure the chemotaxis response that includes the interaction of extracellular PDE and PDI. This response can then be matched to the same response obtained with the microfluidic devices with flowing gradients [21, 22], where the gradient at each cell's position is completely controlled and all secreted molecules (including PDE and PDI)

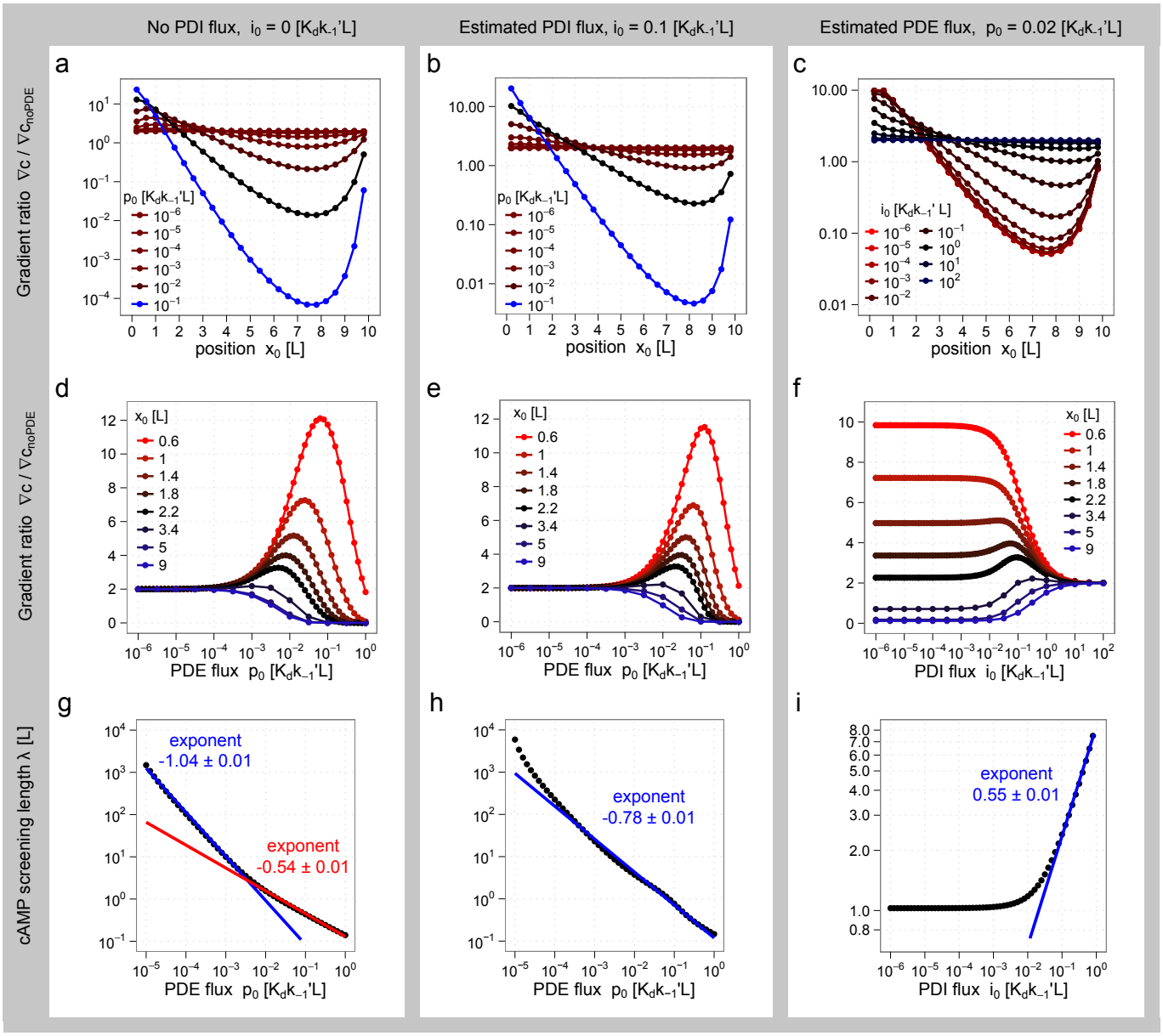

FIG. 3. cAMP gradient ratio across the cell and the cAMP screening length. The left column (a,d,g) represents the results for the model 2 with no PDI flux $i_0 = 0$, the center column (b,e,h) the results with the experimentally estimated value for PDI flux $i_0 = 0.1\, K_d k'_{-1} L$ and the right column the results with the experimentally estimated value for PDE flux $p_0 = 0.02\, K_d k'_{-1} L$. **(a-c)** cAMP gradient ratio across the cell as a function of the distance from the cAMP source. Note that in each case there is a range where the cAMP gradient (and, consequently, cAMP concentration) exhibits an exponential decay which demonstrates the screening effect as discussed in the text. **(d-e)** cAMP gradient ratio across the cell as a function of PDE flux without PDI or with PDI, with cell position x_0 as a parameter. There are two different qualitative regimes: for distances $x_0 \lesssim 5L$ there exists optimal value of PDE flux that maximizes the gradient ratio; for larger distances there is no such behavior and any PDE actually flattens the cAMP gradient. Experimental estimate $p_0 = 0.02\, K_d k'_{-1} L$ is very close to the optimal peak value predicted by the model. **(f)** cAMP gradient ratio across the cell as a function of the PDI flux. There are three qualitatively different regimes: I. sigmoidal behavior for $x_0 \lesssim 1.4L$, II. existence of the optimal PDI flux for $1.4L \lesssim x_0 \lesssim 5L$ and III. flattening of the cAMP gradient for $x_0 \gtrsim 5L$. Both the threshold value and the optimal peak value correspond to the experimental estimate $i_0 = 0.1\, K_d k'_{-1} L$. **(g-h)** Power-law scaling of the cAMP screening length with PDE, with different scaling exponents that distinguish the case (g) with no PDI and (h) with PDI. **(i)** cAMP screening length as a function of PDI flux showing the power-law scaling in the range around its experimental estimate.

are flushed away (see SI for Peclet number arguments). Using both of these results, one could infer the effective cAMP concentration and the gradient in the no-flow system with PDE and PDI present. Since wild-type *D. discoideum* cells secrete cAMP as well, it may be more convenient to use a strain defective in cAMP secretion. Finally, one should not neglect possible and very informative chemotaxis experiments which could be performed with overexpressing PDE and PDI mutants (see e.g. [33]). Using these mutants, one can experimentally vary PDE or PDI secretion rates and search for any of the scaling exponents in the models presented here.

In conclusion, the models presented here show that cells can in principle steepen an external chemical gradient by se-

creting degredatory enzymes. We show that this is a quite significant effect; gradients can be steepened up to a factor of 12. This important effect has been previously neglected in both theoretical models (for a comprehensive review see [34]) and experiments with static non-flowing gradients such as ones in [19, 20, 26], because of the possibility that local gradients may significantly differ from ones in a gradient chamber free of cells. Furthermore, the recently developed microfluidic devices with flowing gradients [21–23] may in fact be destroying these delicate extracellular chemical structures. In the particular example of *D. discoideum* amoebae detecting the cAMP gradient, we find that the experimental secretion rates of PDE (protein that degrades cAMP) and PDI (protein that inhibits PDE) roughly correspond to the optimal values predicted by the second model; see circles in Fig.2.

PDE might have other functions not related to the gradient steepening. For example, Hecht et. al. [35] discussed the problem of amoeboid chemotactic navigation in a maze-like environments and concluded that by secreting its own chemorepellent, amoebae can avoid being trapped and navigate around small obstacles. While such autocrine signaling chemorepellent has not been found, we hypothesize that an extracellular PDE can be used to achieve the same goal.

ACKNOWLEDGMENTS

We thank Cornell ACCEL computer lab for the access to COMSOL Multiphysics and MATLAB software, Archana Rachakonda and Ariana Strandburg-Peshkin for reviewing the manuscript and useful suggestions.

[1] H.C. Berg Motile behavior of bacteria. Phys. Today 53:24-29 (1999)
[2] H.C. Berg and E.M. Purcell, Biophys. J. **20**, 193 (1977)
[3] S.H. Zigmond. Ability of polymorphonuclear leukocytes to orient in gradients of chemotactic factors. J. Cell. Biol. 75:606-616 (1977)
[4] E.T. Roussos, J.S. Condeelis and A. Patsialou, Nat. Rev. Cancer **11**, 573 (2011)
[5] K.F. Swaney, C.H. Huang and P.N. Devreotes, Annu. Rev. Biophys. **39**, 265 (2010)
[6] Y.Y. Chang, Science **161**, 57 (1968)
[7] R.H. Kessin, S.J. Orlow, R.I. Shapiro and J. Franke, Proc. Natl. Acad. Sci. USA **76**, 5450 (1979)
[8] R.H. Kessin, *Dictyostelium: Evolution, Cell Biology and the Development of Multicellularity* (Cambridge University Press, Cambridge, 2001)
[9] N. Barkai, M.D. Rose, N. Wingreen. Protease helps yeast find mating partners. Nature 396:422-423 (1998)
[10] S.S. Andrews, N.J. Addy, R. Brent, A.P. Arkin. Detailed Simulations of Cell Biology with Smoldyn 2.1. PLoS Comp. Biol. 6:e1000705 (2010)
[11] M. Jin, B. Errede, M. Behar, W. Mather, S. Nayak, J. Hasty, H.G. Dohlman, T.C. Elston. Yeast Dynamically Modify Their Environment to Achieve Better Mating Efficiency. Science Signaling 4: ra54 (2011)
[12] V. Nanjundiah and D. Malchow, J. Cell Sci. **22**, 49 (1976)
[13] E. Palsson and E.C. Cox, Proc. Natl. Acad. Sci. USA **93**, 1151 (1996)
[14] E. Palsson, K.J. Lee, R.E. Goldstein, J. Franke, R.H. Kessin and E.C. Cox, Proc. Natl. Acad. Sci. USA **94**, 13719 (1997)
[15] E. Palsson, Biophys. J. **97**, 2388 (2009)
[16] J. Barra, P. Barrand, M.H. Blondelet and P. Brachet, pdsA, a gene involved in the production of active phosphodiesterase during starvation of Dictyostelium discoideum amoebae Mol. Gen. Genet. **177**, 607 (1980)
[17] R. Sucgang, C.J. Weijer, F. Siegert, J. Franke and R.H. Kessin, Null mutations of the Dictyostelium cyclic nucleotide phosphodiesterase gene block chemotactic cell movement in developing aggregates. Dev. Biol. **192**, 181 (1997)
[18] I. Segota, S. Mong, E. Neidich, A. Rachakonda, C. J. Lussenhop and C. Franck, submitted. (2012)
[19] B. Varnum and D.R. Soll, J. Cell Biol. **99**, 1151 (1948)
[20] P.R. Fisher, R. Merkl and G. Gerisch, J. Cell Biol. **108**, 973 (1989)
[21] L. Song, S.M. Nadkarni, H.U. Bodeker, C. Beta, A. Bae, C. Franck, W-J. Rappel, W.F. Loomis and E. Bodenschatz, Eur. J. Cell Biol. **85**, 981 (2006)
[22] D. Fuller, W. Chen, M. Adler, A. Groisman, H. Levine, W-J. Rappel and W.F. Loomis, Proc. Natl. Acad. Sci. USA **107**,9656 (2010)
[23] G. Amselem, M. Theves, A. Bae, C. Beta and E. Bodenschatz, Submitted. (2012)
[24] J.A.M. Borghans, R.J. De Boer and L.A. Segel, Bull. of Math. Biology **58**, 43 (1996)
[25] L. Landau and E. Lifshitz, *Statistical Physics Part 1* (3rd Ed., Pergamon Press, 1976) p.241
[26] S.-Y. Cheng, S. Heilman, M. Wasserman, S. Archer, M.L. Shulerac and M. Wu, Lab Chip **7**, 763 (2007)
[27] S.J. Orlow, R.I. Shapiro, J. Franke and R.H. Kessin, J. Biol. Chem. **256**, 7620 (1981)
[28] C. Beta, T. Frohlich, H.U. Bodeker and E. Bodenschatz, Lab Chip **8**, 1087 (2008)
[29] M. Skoge, M. Adler, A. Groisman, H. Levine, W.F. Loomis and W.-J. Rappel, Integr. Biol. **2**, 659 (2010)
[30] J. Franke and R.H. Kessin, J. Biol. Chem. **256**, 7628 (1981)
[31] M. Dworkin and K. H. Keller, J. Biol. Chem. **252**, 864 (1977)
[32] M. Dworkin and K. H. Keller, "Solubility and diffusion coefficient of adenosine 3':5'-monophosphate", J. Biol. Chem., 252, pp.864-865 (1977)
[33] M. Faure, G.J. Podgorski, J. Franke, R.H. Kessin "Disruption of Dictyostelium discoideum morphogenesis by overproduction of cAMP phosphodiesterase.", Proc. Natl. Acad. Sci. USA, **85** pp.8076-8080 (1988)
[34] A. Bae, Ph.D. thesis, Cornell University, 2011
[35] I. Hecht, H. Levine, W.-J. Rappel and E. Ben-Jacob, PLoS ONE **6**, e21955 (2011)

Supplementary information

Model 1 derivation

As a first and simplest step we only consider the PDE secretion while completely ignoring PDI. We consider a system of two interacting molecules, PDE and cAMP, following a classic Michaelis-Menten kinetics:

$$\text{PDE} + \text{cAMP} \underset{k_{-1}}{\overset{k_1}{\rightleftharpoons}} \text{COMPLEX} \xrightarrow{k_2} \text{PDE} + 5'\text{AMP} \tag{1}$$

where COMPLEX represents the intermediate PDE-cAMP complex and 5'AMP the product of this reaction. 5' AMP does not bind to *Dictyostelium* cAMP receptors and can be considered as a deactivated signal.

We have the following dynamical equations for the concentrations of cAMP $c(x,t)$, PDE $p(x,t)$, cAMP-PDE complex $C_{cp}(x,t)$ and the 5'AMP $c'(x,t)$:

$$\begin{aligned}
\frac{\partial c}{\partial t} &= D_c \nabla^2 c - k_1 cp + k_{-1} C_{cp} \\
\frac{\partial p}{\partial t} &= D_p \nabla^2 p - k_1 cp + (k_{-1} + k_2) C_{cp} \\
\frac{\partial C_{cp}}{\partial t} &= D_{C_{cp}} \nabla^2 C_{cp} + k_1 cp - (k_{-1} + k_2) C_{cp} \\
\frac{\partial c'}{\partial t} &= D_{c'} \nabla^2 c' + k_2 C_{cp}
\end{aligned}$$

where D_c, D_p, $D_{C_{cp}}$ and $D_{c'}$ are the diffusion constants of cAMP, PDE, cAMP-PDE complex and 5'AMP respectively. At this point, it is typical to employ the quasi-steady state assumption [1], which assumes the concentration of the intermediate complex does not change on the time scale of product formation:

$$k_1 cp = (k_{-1} + k_2) C_{cp}$$

$$C_{cp} = \frac{cp}{K_M}, \quad K_M \equiv \frac{k_{-1} + k_2}{k_1}$$

so the equations simplify to:

$$\begin{aligned}
\frac{\partial c}{\partial t} &= D_c \nabla^2 c - k_1 cp + k_{-1} \frac{cp}{K_M} \\
\frac{\partial p}{\partial t} &= D_p \nabla^2 p \\
\frac{\partial C_{cp}}{\partial t} &= D_{C_{cp}} \nabla^2 C_{cp} \\
\frac{\partial c'}{\partial t} &= D_{c'} \nabla^2 c' + k_2 \frac{cp}{K_M}
\end{aligned}$$

and the first equation for cAMP further simplifies to:

$$\frac{\partial c}{\partial t} = D_c \nabla^2 c + cp \left(\frac{k_{-1} - k_1 K_M}{K_M} \right)$$

$$\frac{\partial c}{\partial t} = D_c \nabla^2 c + cp \left(\frac{k_{-1} - k_{-1} - k_2}{K_M} \right)$$

$$\frac{\partial c}{\partial t} = D_c \nabla^2 c - \frac{k_2}{K_M} cp$$

In this model we look at the case where the PDE concentration is uniform in space $p(x) = p_0$, giving us the following equation for cAMP profile in the steady state:

$$D_c \nabla^2 c - \frac{k_2 p_0}{K_M} c = 0$$

In order to make the variables dimensionless, we further make the following substitutions:

$$L \equiv \sqrt{\frac{D_c K_M}{k_2 p_0}}, \ \frac{x}{L} \to x, \ \frac{c}{K_M} \to c$$

and the equation becomes:

$$\nabla^2 c - c = 0 \tag{2}$$

where the cAMP concentration c is now expressed in units K_M, and the spatial coordinate in units of the characteristic length L. Numerically, this length is estimated:

$$L = \sqrt{\frac{D_c K_M}{k_2 p_0}} = \sqrt{\frac{444\ \mu m^2/\mathrm{s} \times 10\ \mu\mathrm{M}}{5000/\mathrm{s} \times 5.2\ \mathrm{nM}}} = 13\ \mu\mathrm{m}$$

1D system

Boundary conditions are taken as $c(x=0) = c_0$ and $c(x=a) = 0$, and we set our system to span ten characteristic lengths, $a = 10$. Physically, this represents a cAMP source at $x = 0$, and a drain "far" away at $x = a$. The equation 2 has the general solution: $c(x) = Ae^x + Be^{-x}$ and with our boundary conditions $c(x=0) = c_0$, $c(x=a) = 0$ we have:

$$\begin{aligned} c(x=0) = A + B = c_0 \qquad & c(x=a) = Ae^a + Be^{-a} = 0 \\ B = c_0 - A \qquad & Ae^a = -Be^{-a} \end{aligned}$$

$$c_0 - A = -Ae^{2a}$$

$$A(e^{-2a} + 1) = c_0$$

$$A = \frac{c_0}{1 - e^{2a}}$$

$$B = c_0 - A = \frac{c_0 - c_0 e^{2a} - c_0}{1 - e^{2a}} = -c_0 \frac{e^{2a}}{1 - e^{2a}}$$

$$c(x) = \frac{c_0}{1 - e^{2a}} e^x + \frac{(-c_0)e^{2a}}{1 - e^{2a}} e^{-x}$$

$$c(x)\frac{1 - e^{2a}}{c_0} = e^x - e^{2a}e^{-x} \not/ \times e^{-a}$$

$$\frac{c(x)}{c_0}\left[e^{-a} - e^a\right] = e^{x-a} - e^{-(x-a)}$$

$$\frac{c(x)}{c_0}\left[-2\sinh(a)\right] = 2\sinh(x-a)$$

$$c(x) = c_0 \frac{\sinh(a-x)}{\sinh(a)}$$

where a is the system size. Without any PDE, the concentration and the gradient are given by:

$$c(x) = c_0\left(1 - \frac{x}{a}\right)$$

$$\frac{dc}{dx} = -\frac{c_0}{a}$$

With uniform PDE, the gradient and the gradient ratio are then:

$$\frac{dc}{dx} = -\frac{c_0 \cosh(a-x)}{\sinh(a)}$$

$$\frac{\nabla c}{\nabla c_{\mathrm{noPDE}}} = \frac{-\frac{c_0 \cosh(a-x)}{\sinh(a)}}{-\frac{c_0}{a}} = \frac{a \cdot \cosh(a-x)}{\sinh(a)}$$

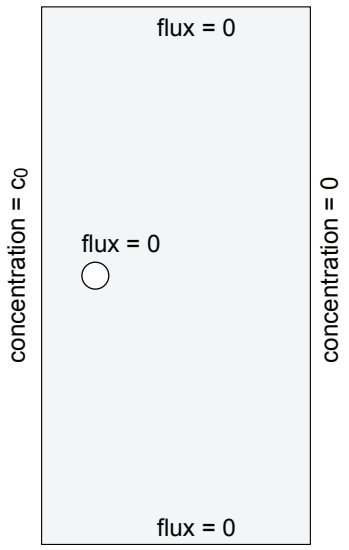

Figure 1: Boundary conditions for cAMP in the Model 1 with uniform PDE concentration.

2D system

2D system was solved by numerically finding the solution of the equation:

$$\nabla^2 c - c = 0 \tag{3}$$

in a system with dimensions of $10L \times 20L$ with the following boundary conditions:

$$\begin{aligned} c(x=0,y) &= c_0 \\ c(x=10,y) &= 0 \\ (-D_c \nabla c)_{x,y=10} &= 0 \\ (-D_c \nabla c)_{x,y=-10} &= 0 \\ (-D_c \nabla c)_{circle} &= 0 \end{aligned}$$

as shown in Fig. 1. The circular boundary models the cell at position $(x, y) = (x_0, 0)$ and as modelled as an insulating boundary with the diffusive flux at its boundary to be zero.

Model 2 derivation, 2D system

We start by writing the dynamical equations for all chemical species $c = [\text{cAMP}]$, $C_{pc} = [\text{COMPLE}X_{pc}]$, $c' = [5\text{'AMP}]$, $p = [\text{PDE}]$, $C_{ip} = [\text{COMPLE}X_{ip}]$ and $i = [\text{PDI}]$ in a 2D system. PDE and PDI sources are modeled as a constant flux boundary at the circle positioned at $(x_0, 0)$ of radius $r = 0.05\,\text{L} \approx 0.05 \times 100\,\mu\text{m} = 5\,\mu\text{m}$:

$$\frac{\partial c}{\partial t} = D_c \nabla^2 c - k_1 cp + k_{-1} C_{pc} \tag{4}$$

$$\frac{\partial C_{pc}}{\partial t} = D_{C_{pc}} \nabla^2 C_{pc} + k_1 cp - (k_{-1} + k_2) C_{pc} \tag{5}$$

$$\frac{\partial c'}{\partial t} = D_{c'} \nabla^2 c' + k_2 C_{pc} \tag{6}$$

$$\frac{\partial p}{\partial t} = D_p \nabla^2 p - k_1 cp + (k_{-1} + k_2) C_{pc} - k'_1 pi + k'_{-1} C_{ip} \tag{7}$$

$$\frac{\partial C_{ip}}{\partial t} = D_{C_{ip}} \nabla^2 C_{ip} + k'_1 pi - k'_{-1} C_{ip} \tag{8}$$

$$\frac{\partial i}{\partial t} = D_i \nabla^2 i - k'_1 pi + k'_{-1} C_{ip} \tag{9}$$

In the quasi steady-state approximation of Michelis-Menten kinetics we take:

$$k_1 cp - (k_{-1} + k_2) C_{pc} = 0$$

from where it follows:

$$C_{pc} = \frac{k_1 cp}{k_{-1} + k_2} = \frac{cp}{K_M}$$

and equations 4-9 simplify to the following:

$$\begin{aligned}
\frac{\partial c}{\partial t} &= D_c \nabla^2 c - \frac{k_2}{K_M} cp \\
\frac{\partial C_{pc}}{\partial t} &= D_{C_{pc}} \nabla^2 C_{pc} \\
\frac{\partial p}{\partial t} &= D_p \nabla^2 p - k'_1 pi + k'_{-1} C_{ip} \\
\frac{\partial C_{ip}}{\partial t} &= D_{C_{ip}} \nabla^2 C_{ip} + k'_1 pi - k'_{-1} C_{ip} \\
\frac{\partial i}{\partial t} &= D_i \nabla^2 i - k'_1 pi + k'_{-1} C_{ip}
\end{aligned}$$

At this point we leave out the equations for c' and C_{pc}, as they are uncoupled from the other equations. In order to make all the variables in these equations dimensionless, we can divide all equations by k'_{-1} (the inverse of the mean time of the dissociation of PDE-PDI complex):

$$\begin{aligned}
\frac{1}{k'_{-1}} \frac{\partial c}{\partial t} &= \frac{D_c}{k'_{-1}} \nabla^2 c - \frac{k_2}{k'_{-1} K_M} cp \\
\frac{1}{k'_{-1}} \frac{\partial p}{\partial t} &= \frac{D_p}{k'_{-1}} \nabla^2 p - \frac{k'_1}{k'_{-1}} pi + C_{ip} \\
\frac{1}{k'_{-1}} \frac{\partial C_{ip}}{\partial t} &= \frac{D_{C_{ip}}}{k'_{-1}} \nabla^2 C_{ip} + \frac{k'_1}{k'_{-1}} pi - C_{ip} \\
\frac{1}{k'_{-1}} \frac{\partial i}{\partial t} &= \frac{D_i}{k'_{-1}} \nabla^2 i - \frac{k'_1}{k'_{-1}} pi + C_{ip}
\end{aligned}$$

and now using the substitutions $k'_{-1} t \to t$ and $k'_{-1}/k'_1 \equiv K_d$ and dividing all equations by K_d:

$$\frac{1}{K_d} \frac{\partial c}{\partial t} = \frac{D_c}{K_d k'_{-1}} \nabla^2 c - \frac{k_2 K_d}{k'_{-1} K_M} \frac{cp}{K_d K_d} \tag{10}$$

$$\frac{1}{K_d} \frac{\partial p}{\partial t} = \frac{D_p}{K_d k'_{-1}} \nabla^2 p - \frac{1}{K_d^2} pi + \frac{1}{K_d} C_{ip} \tag{11}$$

$$\frac{1}{K_d} \frac{\partial C_{ip}}{\partial t} = \frac{D_{C_{ip}}}{K_d k'_{-1}} \nabla^2 C_{ip} + \frac{1}{K_d^2} pi - \frac{1}{K_d} C_{ip}$$

$$\frac{1}{K_d} \frac{\partial i}{\partial t} = \frac{D_i}{K_d k'_{-1}} \nabla^2 i - \frac{1}{K_d^2} pi + \frac{1}{K_d} C_{ip} \tag{12}$$

Using the substitutions $c/K_d \to c,\ p/K_d \to p,\ C_{ip}/K_d \to C_{ip},\ i/K_d \to i$, and simplifying the dimensionless factor in the Eq. 10:

$$\frac{k_2 K_d}{k'_{-1} K_M} = \frac{k_2}{K_M k'_1} \tag{13}$$

we have:

$$\begin{aligned}
\frac{\partial c}{\partial t} &= \frac{D_c}{k'_{-1}} \nabla^2 c - \frac{k_2}{K_M k'_1} cp \\
\frac{\partial p}{\partial t} &= \frac{D_p}{k'_{-1}} \nabla^2 p - pi + C_{ip} \\
\frac{\partial C_{ip}}{\partial t} &= \frac{D_{C_{ip}}}{k'_{-1}} \nabla^2 C_{ip} + pi - C_{ip} \\
\frac{\partial i}{\partial t} &= \frac{D_i}{k'_{-1}} \nabla^2 i - pi + C_{ip}
\end{aligned}$$

$$
\begin{aligned}
\frac{\partial c}{\partial t} &= \frac{D_c}{k'_{-1}}\nabla^2 c - \frac{k_2}{K_M k'_1} cp \\
\frac{\partial p}{\partial t} &= \frac{D_p}{D_c}\frac{D_c}{k'_{-1}}\nabla^2 p - pi + C_{ip} \\
\frac{\partial C_{ip}}{\partial t} &= \frac{D_{C_{ip}}}{D_c}\frac{D_c}{k'_{-1}}\nabla^2 C_{ip} + pi - C_{ip} \\
\frac{\partial i}{\partial t} &= \frac{D_i}{D_c}\frac{D_c}{k'_{-1}}\nabla^2 i - pi + C_{ip}
\end{aligned}
$$

Here we substitute: $x^2 k'_{-1}/D_c \to x^2$ (x)

$$
\begin{aligned}
\frac{\partial c}{\partial t} &= \nabla^2 c - \frac{k_2}{K_M k'_1} cp && (14)\\
\frac{\partial p}{\partial t} &= \frac{D_p}{D_c}\nabla^2 p - pi + C_{ip} && (15)\\
\frac{\partial C_{ip}}{\partial t} &= \frac{D_{C_{ip}}}{D_c}\nabla^2 C_{ip} + pi - C_{ip} && (16)\\
\frac{\partial i}{\partial t} &= \frac{D_i}{D_c}\nabla^2 i - pi + C_{ip} && (17)
\end{aligned}
$$

Using Table 2, we estimate the numerical value of the dimensionless constant in the cAMP equation:

$$K \equiv \frac{k_2}{K_M k'_1} = \frac{5000\ \mathrm{s}^{-1}}{10\times 10^3\mathrm{nM}\ 5\times 10^{-1}\mathrm{nM}^{-1}\mathrm{s}^{-1}} = 1$$

A characteristic length scale related to cAMP is given by $L \sim \sqrt{D_c/k'_{-1}} = \sqrt{(444\mu m^2/\mathrm{s})/(0.05/\mathrm{s})} \approx 100\mu\mathrm{m}$, which is about 10 cell diameters. Another characteristic length scale is $L_2 \sim \sqrt{D_c/(K_M k_1)} = \sqrt{(444\mu m^2/\mathrm{s})/(5000/\mathrm{s})} \approx 0.3\mu m$. This length scale is much smaller than the cell diameter and will not play a significant role in this model. The final set of equations that was solved numerically in steady state is then:

$$
\begin{aligned}
\nabla^2 c &= Kcp && (18)\\
\frac{D_p}{D_c}\nabla^2 p &= pi - C_{ip} && (19)\\
\frac{D_{C_{ip}}}{D_c}\nabla^2 C_{ip} &= -pi + C_{ip} && (20)\\
\frac{D_i}{D_c}\nabla^2 i &= pi - C_{ip} && (21)
\end{aligned}
$$

where the constant K was already estimated to be on the order of 1. The boundary conditions are shown in Fig.2.

For the simpler case where there is no PDI (and consequently PDE-PDI complex), the equations further simplify to:

$$
\begin{aligned}
\nabla^2 c &= Kcp && (22)\\
\nabla^2 p &= 0 && (23)
\end{aligned}
$$

Numerical estmation of diffusion constants

Diffusion constants for PDE, PDI and PDE-PDI complex were estimated using the Stokes-Einstein equation for spherical particles following the approach by Tyn and Gusek [3, 4], who provided the following equation for globular proteins:

$$D[\mathrm{cm}^2/\mathrm{s}] = \frac{9.2\cdot 10^{-8} T[\mathrm{K}]}{\eta[\mathrm{mPas}]\cdot (M_r[\mathrm{Da}])^{1/3}}$$

where T[K] is the absolute temperature in Kelvins, $\eta_{water}^{T=293.15K} = 1\,\mathrm{mPas}$ is the dynamic viscosity of water at 20°C and M_r[Da] molecular mass. The results are given in Table 1.

Biochemical constants

The kinetic parameters used in these models are given in Table 2.

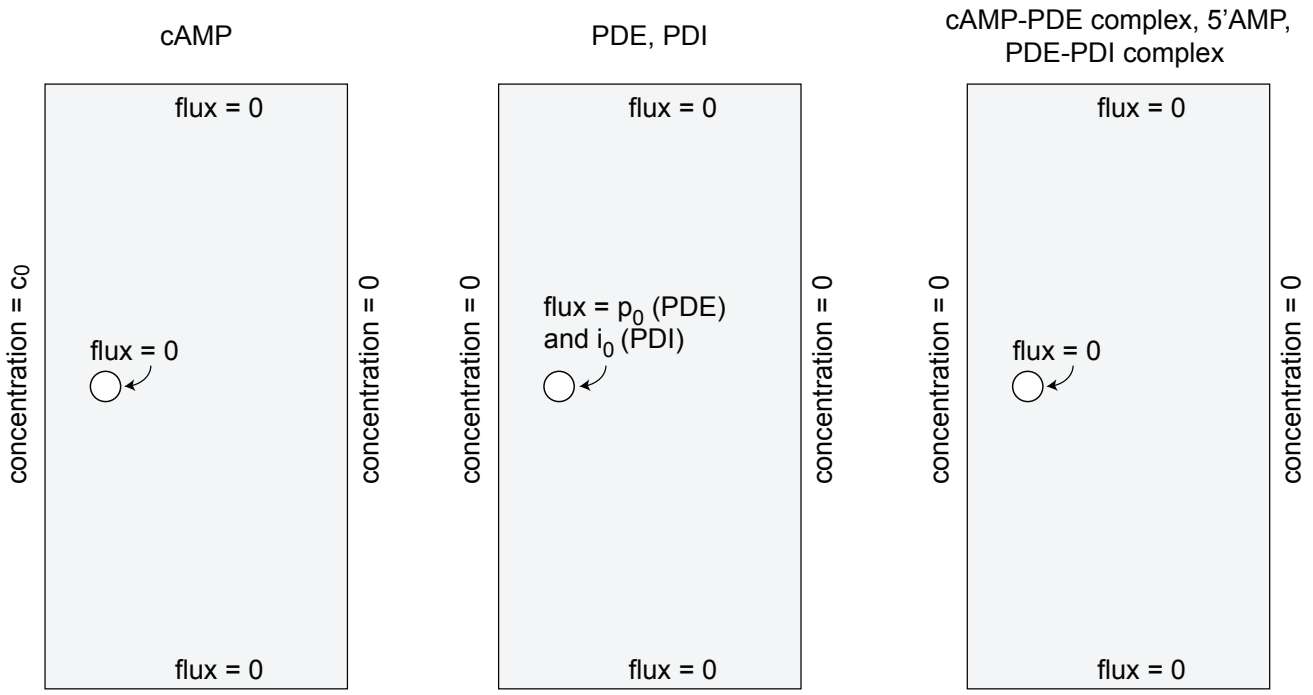

Figure 2: Boundary conditions for Model 2 with a source of PDE and PDI modeled as a constant flux boundary.

	M_r[Da]	$D[\mu m^2/\text{s}]$
PDE	57,500	70
PDI	47,000	74
PDE-PDI complex	104,500	57

Table 1: Estimated diffusion constants of PDE, PDI and PDE-PDI complex.

Numerical estimation of PDE and PDI secretion rates

PDE secretion

In [5], the authors detected 0.6 mg of PDE ($M_r = 55,000-60,000$, so we take 57,500 as the mean) secreted by $N_C = 8\times10^{10}$ cells in $t = 13$ hours (780 min) in 2l suspension volume. The molar quantity of PDE was:

$$\begin{aligned} n &= \frac{m}{M} = \frac{6\times10^{-4}\text{ g}}{57,500\text{ g/mol}} = \frac{6\times10^{-4}\text{g}}{5.75\times10^{4}\text{g/mol}} \\ &= 1.04\times10^{-8}\text{mol} = 10.4\text{ nmol} \end{aligned}$$

and the concentration of PDE in the extracellular environment was (this number is used for Model 1 only):

$$[\text{PDE}] = \frac{n}{V} = \frac{10.4\text{ nmol}}{2\text{ l}} = 5.2\text{ nM}$$

parameter		symbol		value	reference/equation
cAMP diffusion constant		D_c	=	444 μm^2/s	[8]
PDE diffusion constant		D_p	=	70 μm^2/s	estimated
PDI diffusion constant		D_i	=	74 μm^2/s	estimated
PDE-PDI complex diffusion constant		D_{Cip}	=	57 μm^2/s	estimated
PDE-cAMP	Michaelis-Menten constant	K_M	=	10 μM	[9]
	Michaelis-Menten constant	K_M^{app}	=	1 mM (with PDI)	
	association constant	k_1	=	0.5 nM^{-1}s^{-1}	estimated [10]
	turnover number	k_2	=	5000 s^{-1}	$\sim K_M k_1$
PDI-PDE	dissociation constant	K_d	=	0.1 nM	[6]
	dissociation rate	k'_{-1}	=	0.05 s^{-1}	$= k'_1 K_d$
	association rate	k'_1	=	0.5 nM^{-1}s^{-1}	estimated [10]

Table 2: Numerical values for constants. The association constant k_1 and the association rate k'_1 are often limited by the rate of collisions of a diffusing molecule encountering a protein-sized target and typically have values of about $0.1 - 1\,\mathrm{nM}^{-1}\mathrm{s}^{-1}$ [10], so we took the average of $0.5\,\mathrm{nM}^{-1}\mathrm{s}^{-1}$.

The flux due to this secretion is obtained by calculating the molar quantity of PDE molecules passing through the cell surface area (cell being considered a sphere of radius $r = 5\,\mu$m) per unit time:

$$\begin{aligned} p_0(\text{measured}) &\equiv \frac{n/N_C}{A \times t} = \frac{1.3 \times 10^{-10}\ \text{nmol}}{4\pi\,(5\,\mu\text{m})^2 \times 780\,\text{min}} \\ &= \frac{1.3 \times 10^{-19}\text{mol}}{314\,\mu m^2 \times 780\ \text{min}} \\ &= 5.3 \times 10^{-6-19}\,\frac{\text{mol}}{\mu m^2 \text{min}} \\ &= 5.3 \times 10^{-25}\,\frac{\text{mol}}{\mu m^2 \text{min}} \end{aligned}$$

where $(n/N_C)/t$ is the molar quantity of PDE produced by each single cell during the time t. Throughout this model, we use units of $K_d = 0.1\,$nM for concentrations, characteristic length scale $L = 100\,\mu$m for lengths and $1/k'_{-1} = 20\,$s for times. Dissociation constant is then:

$$\begin{aligned} 1\,K_d &= 10^{-10}\,\frac{\text{mol}}{\text{l}} = 10^{-10}\,\frac{\text{mol}}{10^{15}\mu m^3} \\ &= 10^{-25}\,\frac{\text{mol}}{\mu m^3} \end{aligned}$$

In these units, the PDE flux is:

$$\begin{aligned} p_0(\text{measured}) &= 5.3 \times 10^{-25}\,\frac{\text{mol}\mu\text{m}}{\mu m^3 \text{min}} \\ &= 5.3\,\frac{K_d \times 10^{-2} L}{3\left(1/k'_{-1}\right)} \\ &= 1.76 \times 10^{-2}\,K_d k'_{-1} L \\ &= 17.6 \times \left(10^{-3}\,K_d k'_{-1} L\right) \\ &\approx 0.02\,K_d k'_{-1} L \end{aligned}$$

With $K_d = 0.1\,\mathrm{nM}$, $k'_{-1} = 0.05\,\mathrm{s}^{-1}$ and $L = 100\,\mu\mathrm{m}$:

$$\begin{aligned} K_d k'_{-1} L &= \frac{0.1 \times 10^{-9}\mathrm{mol}}{10^{15}\,\mu\mathrm{m}^3} \cdot 0.05\,\mathrm{s}^{-1} \cdot 10^2\,\mu\mathrm{m} \\ &= 10^{-1-9-15} \cdot 6 \cdot 10^{23} \cdot 5 \cdot 10^{-2} \cdot 10^2\,\frac{\mathrm{molecules}}{\mu\mathrm{m}^2 \cdot \mathrm{s}} \\ &= 30 \cdot 10^{-2}\,\frac{\mathrm{molecules}}{\mu\mathrm{m}^2 \cdot \mathrm{s}} \\ &= 0.3\,\frac{\mathrm{molecules}}{\mu\mathrm{m}^2 \cdot \mathrm{s}} \end{aligned}$$

PDI secretion

In [6], the authors note that PDI activity was 500 units/ml, that 2500 units of PDI correspond to about 0.12 nmol (with $M_r = 47,000$), and that the cell density was $c_C = 2.6 \times 10^7$ cells/ml. The concentration of PDI in the extracellular medium is therefore:

$$[\mathrm{PDI}] = 500\,\frac{\mathrm{units}}{\mathrm{ml}} \times \frac{0.12\ \mathrm{nmol}}{2500\ \mathrm{units}} = 0.024\,\frac{\mathrm{nmol}}{\mathrm{ml}} = 24\,\mathrm{nM}$$

Total molar quantity of PDI in the entire volume was:

$$n = [\mathrm{PDI}] \times V = 0.024\,\frac{\mathrm{nmol}}{\mathrm{ml}} \times 700\ \mathrm{ml} = 16.8\ \mathrm{nmol}$$

We can also estimate the PDI concentration by a different method. Using the experimental fact that the PDI acts as a competitive inhibitor [6], we can estimate the concentration of PDI using the equation for the apparent K_M^{app} [7]:

$$K_M^{app} = K_M \left(1 + \frac{[\mathrm{PDI}]}{K_d}\right)$$

and given $K_M^{app} = 1\mathrm{mM}$, $K_M = 10\mu\mathrm{M}$ and $K_d = 0.1\mathrm{nM}$ (see Table 2), we obtain:

$$\frac{K_M^{app}}{K_M} = 1 + \frac{[\mathrm{PDI}]}{K_d}$$

$$\begin{aligned} [\mathrm{PDI}] &= K_d \left(\frac{K_M^{app}}{K_M} - 1\right) = 0.1\ \mathrm{nM} \left(\frac{10^3\mu\mathrm{M}}{10\mu\mathrm{M}} - 1\right) \\ &\approx 10\ \mathrm{nM} \end{aligned}$$

which is relatively close to the previous rough estimate of 24 nM. Here we take the average of these two values to obtain 17 nM. The corresponding value for the molar quantity of PDI is $n = 17\mathrm{nM} \times 0.7\mathrm{l} \approx 12$ nmol. The total cell number was:

$$N_C = c_C V = 2.6 \times 10^7\ \frac{\mathrm{cells}}{\mathrm{ml}} \times 700\ \mathrm{ml} = 1.82 \times 10^{10}\ \mathrm{cells}$$

Since the cells were starved and produced PDI for about 13 hours (780 minutes), the PDE flux for each cell is:

$$\begin{aligned} i_0(\mathrm{measured}) &\equiv \frac{n/N_C}{A \times t} = \frac{6.6 \times 10^{-10}\ \mathrm{nmol}}{4\pi\,(5\,\mu\mathrm{m})^2 \times 780\,\mathrm{min}} \\ &= \frac{6.6 \times 10^{-10}\mathrm{mol}}{314\,\mu m^2 \times 780\ \mathrm{min}} \\ &= 2.7 \times 10^{-5-19}\,\frac{\mathrm{mol}}{\mu m^2 \mathrm{min}} \\ &= 27 \times 10^{-25}\,\frac{\mathrm{mol}}{\mu m^2 \mathrm{min}} \end{aligned}$$

In our units of $K_d = 0.1\,\mathrm{nM}$ for concentrations, characteristic length scale $L = 100\,\mu\mathrm{m}$ for lengths and $1/k'_{-1} = 20\,\mathrm{s}$ for times, the PDI flux is (with $1\,K_d = 10^{-25}\mathrm{mol}/\mu m^3$):

$$\begin{aligned} i_0(\text{measured}) &= 27 \times 10^{-25}\,\frac{\mathrm{mol}\mu\mathrm{m}}{\mu m^3 \mathrm{min}} \\ &= 27\,\frac{K_d \times 10^{-2} L}{3\left(1/k'_{-1}\right)} \\ &= 9 \times 10^{-2}\,K_d k'_{-1} L \\ &= 90 \times \left(10^{-3}\,K_d k'_{-1} L\right) \\ &\approx 0.1\,K_d k'_{-1} L \end{aligned}$$

Finite Element Method

We solved the set of differential equations 18-21 using Finite Elements Method, where we used COMSOL Multiphysics v3.5 (Comsol Inc.) using the custom script that connects to COMSOL through the MATLAB interface. We used Chemical Engineering / Diffusion module, specified the model numerically in MATLAB, then found the steady-state solutions using the built-in stationary solver. The domain was meshed with triangular domains where the maximum mesh size was chosen at most 0.5 L. Depending on the model parameters, COMSOL could not occassionaly found a solution with 0.5 L mesh size, so for those cases we lowered to either 0.1 L or 0.5 L. An example of typical meshing with 0.5 L maximum mesh size is shown in Fig.3. We used stationary non-linear PDE solver `femstatic()` to find the solution. The data was further analyzed and plotted in R [11].

Calculation of cAMP screening lengths and its scaling

The cAMP gradient ratio was log-transformed and an exponential length was found by a linear least-square fit between log-transformed cAMP gradient ratio and the position, x_0.

cAMP screening length as a function of PDE flux in the case of no PDI was fit to power laws, as follows: the values $10^{-5}\,K_d k'_{-1} L \le p_0 \le 4 \cdot 10^{-3}\,K_d k'_{-1} L$ were fit to one exponent and $4 \cdot 10^{-3}\,K_d k'_{-1} L \le p_0 \le 10^{0}\,K_d k'_{-1} L$ to second exponent, and for both we estimated the exponential screening length in the spatial range $1 \le x_0/L \le 6$.

cAMP screening length as a function of PDI flux was calculated for values $1 \le x_0/L \le 6$ and $10^{-6}\,K_d k'_{-1} L \le i_0 \le 10^{0}\,K_d k'_{-1} L$ and a line was fit on a log-log plot for the range $0.08\,K_d k'_{-1} L \le i_0 \le 1\,K_d k'_{-1} L$, with the slope 0.55 ± 0.01 indicating a possible power law scaling.

Effects of cell size

We estimated the effects of cell size on the gradient perceived by the cell in the same way as authors in [12]. We also estimated the gradient enhancement by a factor of two is due to the effects of cell shape as shown in Fig. 4.

Peclet number arguments for flowing gradient experiments

Peclet number is a dimensionless measure of the ratio of the advective to diffusive transport, defined by:

$$Pe = \frac{vl}{D}$$

where D is the diffusion coefficient of the molecule in question, v the flow velocity and l the characteristic length. For a cAMP diffusion with diffusion coefficient of about $400\,\mu\mathrm{m}^2/\mathrm{s}$, typical flow rates around $600\,\mu\mathrm{m}/\mathrm{s}$, so the diffusion dominates ($Pe \ll 1$) only for length scales $l \ll 1.5\,\mu\mathrm{m}$.

References

[1] J.A.M. Borghans, R.J. De Boer and L.A. Segel, "Extending the Quasi-Steady State Approximation by Changing Variables", Bull. of Math. Biology, 58, pp. 43-63, (1996)

[2] http://mathworld.wolfram.com/ModifiedBesselDifferentialEquation.html

[3] G. Carta, A. Jungbauer, "Protein Chromatography: Process Development and Scale-Up", Wiley-WCH, p.36 (2010)

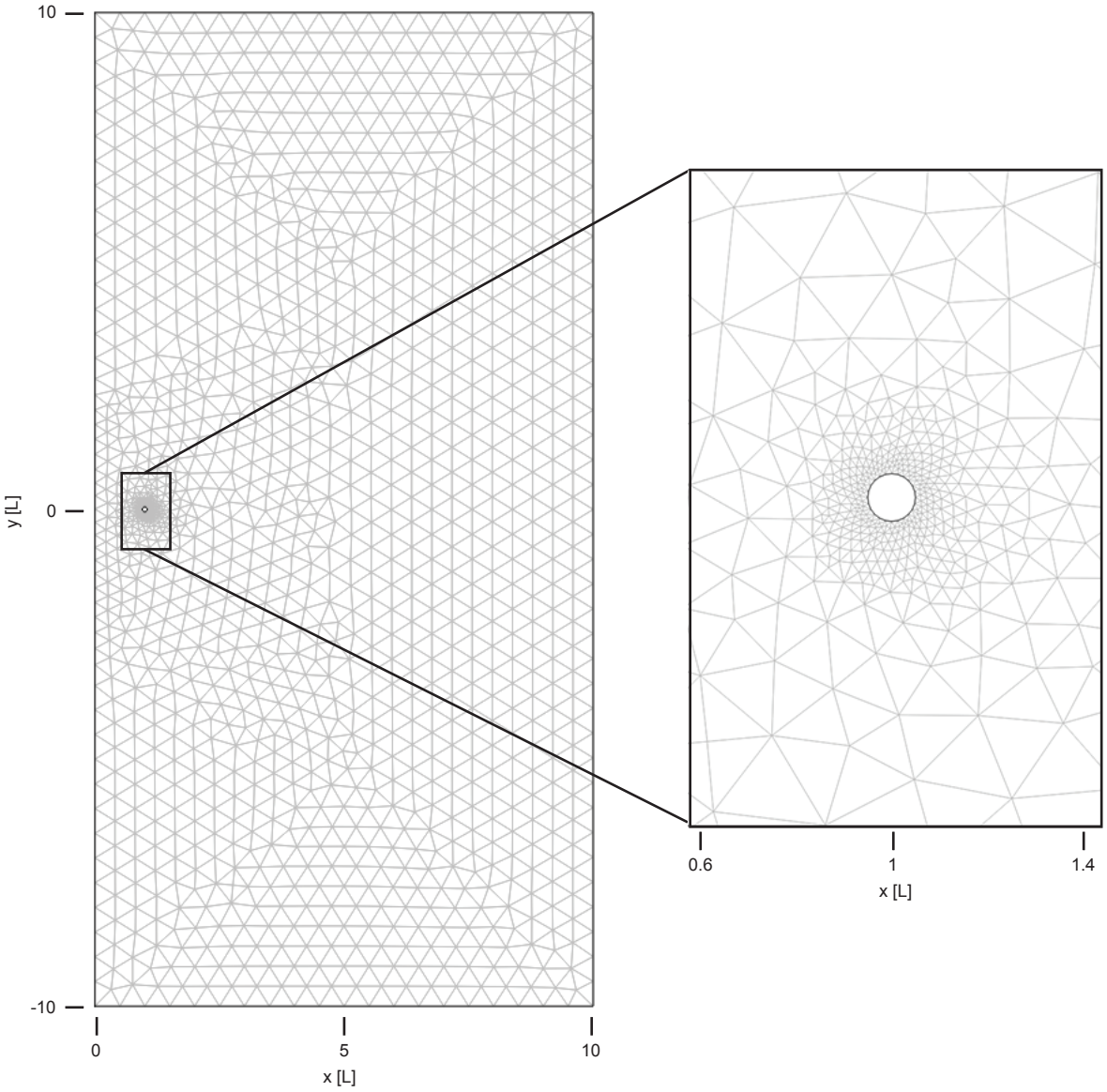

Figure 3: An example of mesh used for Finite Element Method calculations.

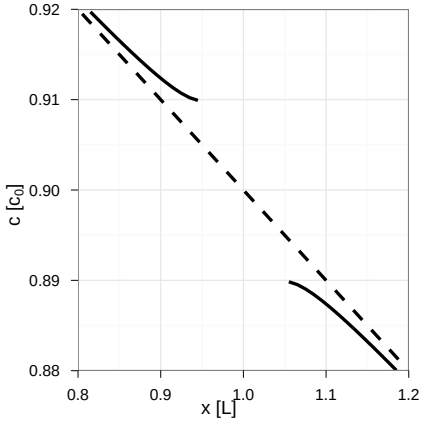

Figure 4: Effect of cell size on the perceived gradient. The actual cAMP concentration, modeled as an insulating boundary, is shown with a solid line, while the linear cAMP concentration in the absence of a cell is shown as a dashed line.

[4] M.T. Tyn, T.W. Gusek, “Prediction of Diffusion Coefficients of Proteins”, Biotechnol. Bioeng., 35, pp.327-338 (1989)

[5] S.J. Orlow, R.I. Shapiro, J. Franke and R.H. Kessin, “The Extracellular Cyclic Nucleotide Phosphodiesterase of Dictyostelium discoideum”, J. Biol. Chem., 256, pp.7620-7627 (1981)

[6] J. Franke and R.H. Kessin, ”The Cyclic Nucleotide Phosphodiesterase Inhibitory Protein of Dictyostelium discoideum”, J. Biol. Chem., 256, pp.7628-7637 (1981)

[7] J.M. Berg, J.L. Tymoczko and L. Stryer, “Biochemistry”, W.H. Freeman and Company, New York, first ed., p.226

[8] M. Dworkin and K. H. Keller, “Solubility and diffusion coefficient of adenosine 3’:5’-monophosphate”, J. Biol. Chem., 252, pp.864-865 (1977)

[9] R.H. Kessin, S.J. Orlow, R.I. Shapiro and J. Franke, “Binding of inhibitor alters kinetic and physical properties of extracellular cyclic AMP phosphodiesterase from Dictyostelium discoideum”, Proc. Natl. Acad. Sci. USA, 76, pp. 5450-5454 (1979)

[10] U. Alon, “Introduction to systems biology”, Chapman & Hall CRC, p.242 (2007)

[11] R Core Team, “R: A Language and Environment for Statistical Computing”, Vienna, Austria (2012) `http://www.R-project.org`

[12] M. Skoge, M. Adler, A. Groisman, H. Levine, W.F. Loomis and W.-J. Rappel, “Gradient sensing in defined chemotactic fields”, Integr. Biol., 2, pp.659-668 (2010)